# Fiber Type and Subcellular-Specific Analysis of Lipid Droplet Content in Skeletal Muscle

**Camille M. Selvais**[1], **Laura L. De Cock**[1], **Sonia M. Brichard**[1], **María A. Davis-López de Carrizosa**[1,2]

[1] Endocrinology, Diabetes and Nutrition Unit, Institute of Experimental and Clinical Research, Medical Sector, Université Catholique de Louvain  [2] Departamento de Fisiología, Facultad de Biología, Universidad de Sevilla

## Corresponding Author

**María A. Davis-López de Carrizosa**

mayadavis@us.es

## Abstract

Skeletal muscle lipid infiltration, known as myosteatosis, increases with obesity and ageing. Myosteatosis has also recently been discovered as a negative prognostic factor for several other disorders such as cardiovascular disease and cancer. Excessive lipid infiltration decreases muscle mass and strength. It also results in lipotoxicity and insulin resistance depending on total intramyocellular lipid content, lipid droplet (LD) morphology, and subcellular distribution. Fiber type (oxidative vs glycolytic) is also important, since oxidative fibers have a greater capacity to utilize lipids. Because of their crucial implications in pathophysiology, in-depth studies on LD dynamics and function in a fiber type-specific manner are warranted.

Herein, a complete protocol is presented for the quantification of intramyocellular lipid content and analysis of LD morphology and subcellular distribution in a fiber type-specific manner. To this end, serial muscle cryosections were stained with the fluorescent dye Bodipy and antibodies against myosin heavy chain isoforms. This protocol enables the simultaneous processing of different muscles, saving time and avoiding possible artifacts and, thanks to a personalized macro created in Fiji, the automatization of LD analysis is also possible.

## Introduction

Skeletal muscle lipid infiltration, known as myosteatosis, increases with obesity and ageing. Myosteatosis is negatively correlated with muscle mass and strength and with insulin sensitivity[1]. Moreover, recent studies indicate that the degree of myosteatosis could be used as a prognostic factor for other conditions such as cardiovascular disease[2], non-alcoholic fatty liver disease[3], or cancer[4]. Lipids can accumulate in

skeletal muscle between muscle fibers as extramyocellular lipids or within the fibers, as intramyocellular lipids (IMCLs). IMCLs are predominantly stored as triglycerides in lipid droplets (LDs) that are used as metabolic fuel during physical exercise[5,6]. However, when lipid supply exceeds demand, or when mitochondria become dysfunctional, IMCLs will be implicated in muscle insulin resistance, as seen

in metabolically unhealthy, obese individuals and in type 2 diabetes patients[7]. Intriguingly, endurance athletes have similar, if not higher, levels of IMCLs to those found in obese patients with type 2 diabetes mellitus, while maintaining high insulin sensitivity. This phenomenon is described as the "athlete's paradox"[8,9], and is explained by a more nuanced appraisal of muscle LDs, related to their size, density, localization, dynamics, and lipid species composition.

First, LD size is inversely correlated to insulin sensitivity and physical fitness[10,11]. In fact, smaller LDs exhibit a relatively greater surface area for lipase action and, thus, potentially have a greater capacity to mobilize lipids[12]. Second, LD density (number/surface) plays a controversial role in insulin action[8,10]; yet, it seems to be increased in athletes. Third, the subcellular localization of LDs is important, since LDs located just below the surface membrane (subsarcolemmal or peripheral) exert a more deleterious effect on insulin sensitivity than central ones[8,9,13]. The latter provide fuel to central mitochondria, which have a greater respiratory activity and are more specialized to meet the high energy demand required for contraction[14]. By contrast, peripheral LDs supply subsarcolemmal mitochondria, which are involved in membrane-related processes[8]. Finally, beyond triglycerides, specific complex lipids within the muscle may be more deleterious than others. For instance, diacylglycerol, long-chain acyl-CoA, and ceramides may accumulate in muscle when the triglyceride turnover rate is low, thereby impairing insulin signaling[9,15]. Returning to the "athlete's paradox," endurance athletes have a high number of smaller central LDs with elevated turnover rates in type I (oxidative) fibers, while obese and diabetic patients have larger peripheral LDs with low turnover rates in type II (glycolytic) fibers[8,15,16]. In addition to their role in energy storage and release, LDs *via* derived fatty acids (FA) and a coat protein (perilipin 5) could

also function as critical players involved in the transcriptional regulation of FA oxidation and mitochondrial biogenesis[8]. Because of their crucial implications in physiology and pathophysiology, in-depth studies on LDs dynamics and functions are warranted.

Although there are several techniques to study IMCLs, they are not all suitable to accurately quantify LD size, density, and distribution in a fiber-specific manner. For example, the assessment of IMCLs by magnetic resonance spectroscopy, while being non-invasive, offers a level of resolution that is not sufficient to study the size and precise location of LDs within the fiber, and it is not fiber-type specific[17,18]. Likewise, biochemical techniques performed on whole-muscle homogenates[19] cannot assess the location and size of lipids. Consequently, the most adequate method to analyze LD morphology and location is quantitative transmission electronic microscopy[13], but this technique is expensive and time-consuming. Therefore, confocal fluorescence imaging on preparations with dyes such as Oil Red O (ORO)[20,21], monodansylpentane (MDH)[22], or Bodipy[23,24,25], has emerged as the best tool for these studies.

Here, a complete protocol is described, including tissue sampling and processing, Bodipy staining, and confocal image acquisition and analysis to quantify LD size, number, and localization in mouse muscle cryosections. Since IMCLs are not evenly distributed among oxidative and glycolytic fibers, and each fiber type regulates LD dynamics differently, the study of IMCLs must be fiber-type specific[16,25,26,27]. Therefore, this protocol uses immunofluorescence on serial sections to identify myosin heavy chain (MyHC) isoform(s) expressed by each fiber. Another advantage of this protocol is the simultaneous processing of a glycolytic

(extensor digitorum longus, EDL) and an oxidative (soleus) muscle placed side-by-side before freezing (**Figure 1**). This simultaneous processing not only saves time but also avoids variability due to separate processing of the samples.
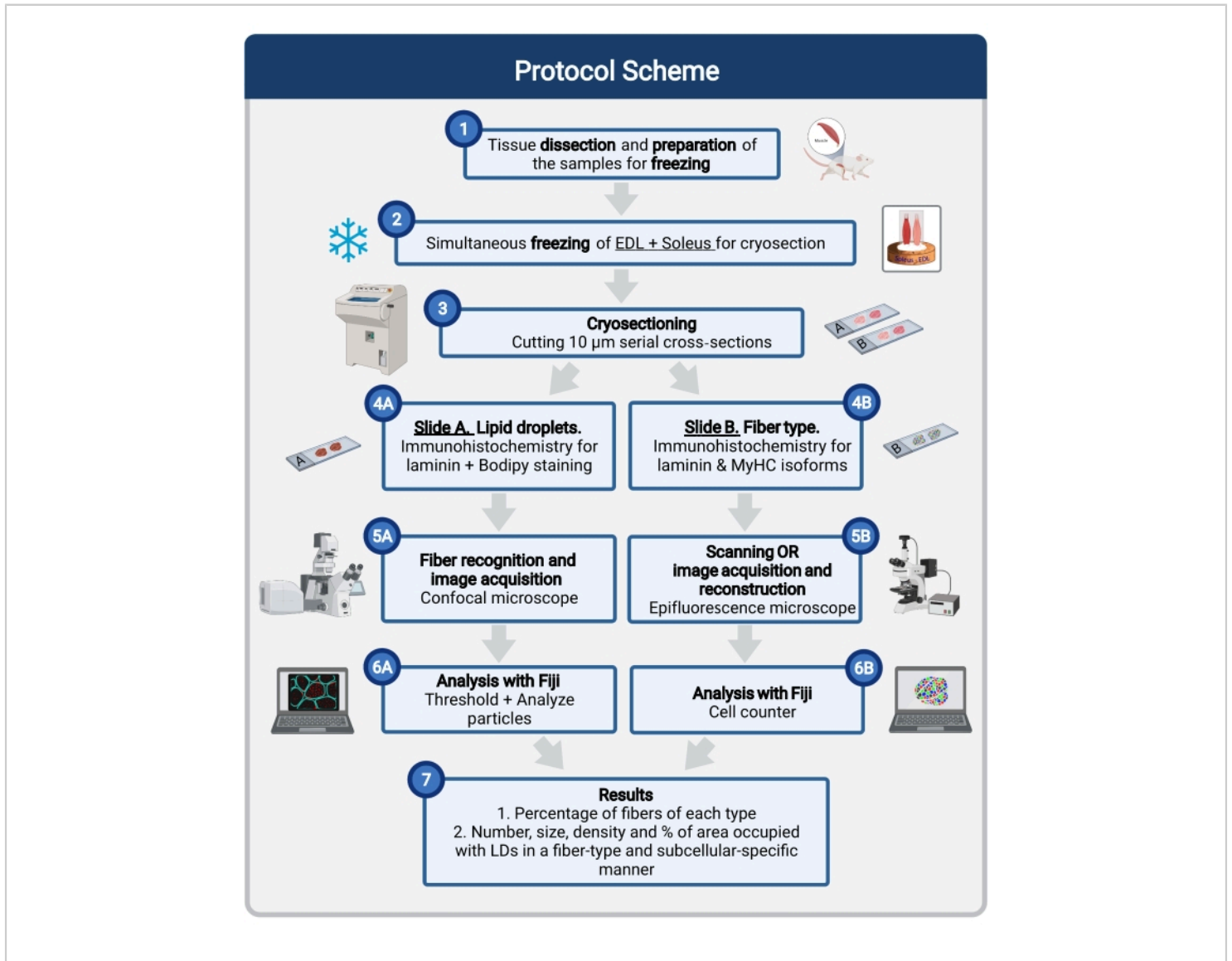


**Figure 1: Schematic overview of the procedure.** After muscle dissection (1), similar-size selected muscles are prepared and frozen together (2). Serial transverse sections of 10 μm are obtained using a cryostat and directly mounted on adhesion slides (3). From two serial slides, the first (4A) is immunolabeled for laminin and stained with Bodipy to recognize LDs and the second (4B) is immunostained with antibodies against MyHCs for the recognition of muscle fiber types. Images are acquired using a confocal microscope for Bodipy (5A) and an epifluorescence microscope for muscle fiber types (5B). Images are analyzed in Fiji by applying a threshold and quantifying particles (6A) to obtain the number, average size, density, and percentage of the total area occupied by LDs (7) or counting cells (6B) to obtain the percentage of fibers of each

type in the section (7). Abbreviations: LDs = lipid droplets; EDL = extensor digitorum longus; MyHCs = myosin heavy chain isoforms. Please click here to view a larger version of this figure.

## Protocol

All procedures conducted on mice were approved by the Ethical Committee for Animal Experimentation from the Medical Sector at Université Catholique de Louvain (2019/UCL/MD/013).

### 1. Dissection and preparation of the samples for freezing

1. Label a 3 mm thick piece of cork for each pair of muscles.

2. Through a small incision made with a blade on the center of the cork, insert perpendicularly a rectangular piece of rigid plastic (0.5 cm W, 1 cm H) that will serve as support (**Figure 2B**).
   NOTE: The size of the rectangular plastic piece will depend on the size of the muscle. Here, the described dimensions are adapted to the size of the soleus (~9 mg, 1 cm L, 2-3 mm W) and EDL (~5 mg, 1 cm L, 2-3 mm W) of a 3-month-old C57BL/6J male mouse.

3. At the time of dissection, remove the soleus and EDL of the mouse hind limb. To prevent the samples from drying out during dissection, place them on a compress lightly moistened with saline solution in a Petri dish placed on ice.
   NOTE: See Wang et al.[28] for explanations on how to dissect these two limb muscles.

4. Place a small drop of Optimal Cutting Temperature compound (OCT) at the cork/plastic junction, avoiding air bubbles.

5. Eliminate excess moisture from the samples by gently drying them with a paper towel (**Figure 2A**) and place both muscles on the plastic perpendicular to the cork (**Figure 2C**).

6. Check the orientation of the muscle myofibers under a stereo microscope (**Figure 2D**).
   NOTE: It is important not to cover the muscle with OCT, since its insulating effect would prevent rapid freezing and will produce freezing artifacts.

### 2. Freezing skeletal muscle samples for cryosectioning

CAUTION: Freezing of the muscle must be done under a chemical hood, wearing appropriate personal protective equipment (see the **Table of Materials**).

1. Use a stainless-steel tumbler (~8 cm H, 6 cm Ø) with two side straps attached to it at least 25 cm long (**Figure 2F**), and fill the tumbler up to 2/3 of its capacity with isopentane.

2. Grabbing the tumbler by the straps, immerse it gently in a polystyrene box filled with liquid nitrogen so that the level of nitrogen outside the container is above the level of isopentane inside (**Figure 2F,G**).
   CAUTION: When the tumbler comes into contact with the nitrogen, the thermal shock may cause swirling. Ensure that the tumbler is sufficiently immersed but avoid the entry of nitrogen as this would cause isopentane precipitation. If this happens, let the isopentane cool down, fill the tumbler with new isopentane and start over.

3. When the inside of the tumbler is completely covered with a white solid layer of isopentane, take it out of the liquid nitrogen box (**Figure 2H**).

   NOTE: The melting temperature of isopentane being -159 °C, the edges of the tumbler will turn white when it is cold enough.

4. Gently stir the solid isopentane pieces into the remaining liquid isopentane with forceps until the entire volume becomes liquid again.

5. Re-immerse the tumbler in the liquid nitrogen until isopentane forms white pebbles all over the bottom and edges of the tumbler (**Figure 2G,H**).

   NOTE: This second cooling step ensures the appropriate freezing temperature of the isopentane.

6. Remove the tumbler from the liquid nitrogen and quickly dip the muscles in the bottom of the tumbler, holding the cork with rat tooth tweezers. Swirl the cork for 15 s in the isopentane and store it at -80 °C until processing (**Figure 2I**).

   NOTE: For short-term storage, the samples can be maintained in a -20 °C freezer. The complete protocol for rapid freezing of skeletal muscle has already been published elsewhere. For detailed references and troubleshooting, see: Meng et al.[29], Kumar et al.[30], and Leiva-Cepas et al.[31].

## 3. Cryosectioning

1. Bring the samples into the chamber of a cryostat previously cooled to -20 °C and the blade temperature set to -25 °C.

   NOTE: Transport samples from the -20 °C/-80 °C freezer to the cryostat in a polystyrene box filled with dry ice and allow the samples to equilibrate for at least 20-30 min to the chamber temperature before cutting.

2. Remove the plastic from the cork with fine tweezers and place the cryostat specimen disc on the quick freeze plate to cool. Once the plate has reached -50 °C, place some OCT on the disc and quickly place the cork on top of the disk, pressing firmly. Wait until the OCT solidifies and the cork is well fixed on the disc.

3. Place the disc on the object head in the desired cutting orientation (**Figure 2J,K**) and trim the muscle block beyond at least 1/3 of the length of the muscles and until both cross sections of the muscles are visible.

4. Set the cutting thickness to 10 µm and place one section on an adhesion slide to check the correct orientation of the fibers on a brightfield microscope.

   NOTE: Checking the transverse orientation of the fibers is critical. If the fibers are not adequately oriented, adjust the angle of the object head, cut another section and check again.

5. Place two serial cross-sections on two prelabeled adhesion slides: one slide to determine fiber types, the other to quantify lipid content (**Figure 2L**).

   NOTE: Additional serial cross sections can be obtained and kept at -80 °C for other histological studies. However, to avoid altering the lipid content and intracellular morphology[24], it is essential to process the first two slides immediately after cutting to prevent air-drying. Freezing and thawing the slides for LD quantification would have the same effect and is thus highly inadvisable.

## 4. Fiber typing and Bodipy staining

1. Immunohistochemical detection of muscle fiber type

NOTE: For the following protocol, a total solution volume of 250 µL is sufficient to cover the entire muscle section surrounded by a circle drawn with a hydrophobic pen the approximate size of a 1 cent coin.

1. Surround the sections with an outline drawn with a hydrophobic pen and rinse with ice-cold 0.1 M phosphate-buffered saline (PBS) for 1 min at room temperature (RT). Place the slide in a humid chamber and block for 90 min at 37 °C in blocking solution (10% normal goat serum (NGS) and 1:30 mouse on mouse (MOM) blocking reagent in PBS).

2. Remove the blocking solution and incubate the slides for 90 min at 37 °C with the solution containing the primary antibodies (5% NGS, 1:30 MOM blocking reagent, the mouse primary antibodies to recognize type I (IgG2b, at 1:10), type IIa (IgG1, at 1:10), and type IIx (IgM, at 1:5) fibers and a rat anti-laminin (α2 chain, 1:1,000) in PBS.

3. Wash the slides with PBS 3 x 5 min at RT.

4. Incubate the slides in the dark for 1 h at RT with the solution containing the secondary antibodies (goat anti-IgG2b AF405 (1:500), goat anti-IgG1 AF488 (1:500), goat anti-IgM AF568 (1:1,000), and goat anti-laminin AF647 (1:500) in PBS).
   CAUTION: For the rest of the protocol, make sure to keep the slides away from light to preserve the fluorescence.

5. Wash again 3 x 5 min in PBS, rinse in double-distilled H$_2$O, remove excess water, and mount with an antifade reagent.
   NOTE: Store the slides at 4 °C, protected from light to preserve the fluorescence until image acquisition. Since the slides are not fixed, it is recommended

to use freshly made solutions for each experiment, autoclave the PBS, and acquire the images as soon as possible to avoid contamination of the sections.

2. Staining of LDs with Bodipy

NOTE: Similar to step 4.1., a total solution volume of 250 µL is sufficient to cover the entire muscle section surrounded by a circle drawn with a hydrophobic pen the approximate size of a 1 cent coin.

1. Surround the sections with an outline drawn by a hydrophobic pen and rinse with ice-cold 0.1 M PBS for 10 min at RT. Use ice-cold PBS for all the rinses and washes.

2. Fix with cold 4% paraformaldehyde (PFA) without methanol for 10 min at RT. After a first quick rinse, wash the slides with PBS 3 x 5 min at RT.
   CAUTION: Perform this step under a chemical hood.

3. Place the slide in a humid chamber and block for 1 h at RT with 5% NGS in PBS.

4. Incubate the slides for 90 min at 37 °C with the solution of the primary antibody (2% NGS and rat anti-laminin (α2 chain, 1:1,000) in PBS). Wash the slides with PBS 3 x 5 min at RT.
   CAUTION: For the rest of the protocol, make sure to keep the slides away from light to preserve the fluorescence.

5. Incubate for 1 h at RT with the secondary antibody solution containing goat anti-rat-AF647 antibody (1:500) in PBS. Wash the slides with PBS 3 x 5 min at RT.

6. Incubate for 20 min at RT with a solution of 4',6-diamidino-2-phenylindole (DAPI, 0.5 µg/mL) and BODIPY (1 µg/mL) in PBS.

NOTE: To prepare BODIPY stock solution, dissolve it in DMSO at a concentration of 1 mg/mL. Different Bodipy formulations are commercially available for LD staining. Depending on the choice made, the staining method is the same (same steps, concentration, and incubation time); however, the acquisition method will be slightly different.

7. After a first quick rinse, wash the slides with PBS 3 x 5 min at RT, rinse in double-distilled $H_2O$, remove excess water, and mount with an antifade reagent.

   NOTE: Store the slides at 4 °C, protected from light, to preserve the fluorescence until image acquisition.

## 5. Acquisition of images

NOTE: Once the staining protocols have been completed, it is important to proceed immediately to image acquisition (within the following 24 h), not only to avoid contamination but also to preserve the morphology, size, and number of LDs.

1. Acquisition of images to assess the fiber-types of each muscle sampled

   NOTE: This step could be achieved with a whole-slide fluorescence scanning microscope or with a conventional epifluorescence microscope. With the latter, manual or automated stitching of the images must be done to reconstruct the section.

   1. For fiber-type recognition, use an epifluorescence microscope with a 10x/0.3 objective. Select excitation filters for DAPI (405 nm), FITC, TRITC, and Cy5 to detect type I, IIa, IIx fibers, and laminin, respectively.

      NOTE: Type IIb fibers will not be immunolabeled. They will be recognized as fibers stained by laminin

on the limits of the sarcolemma with a black sarcoplasm.

   2. Adjust the appropriate exposure time for each channel.

   3. When using a conventional epifluorescence microscope, always acquire the images of the entire muscle following the same order to facilitate muscle reconstruction. Make sure that the fibers on the right edge of one image also appear on the left edge of the following image. The same applies for the top and the bottom parts of the images (**Figure 3A**).

      NOTE: As a reference, for a section of the EDL or the soleus dissected from a 3-month-old mouse, an average of six and eight images, respectively, will cover the entire muscle cross-section.

   4. After the muscle is scanned, upload the captured digital images into any image-processing software for reconstruction (stitching), based on the fiber morphology (laminin) and the histology of the muscle section, and save it as a TIFF, PNG, or JPG file with all the channels (colors) merged (**Figure 3A**).

2. Acquisition of images with laminin and Bodipy co-staining

   NOTE: To recognize the fiber type and have an estimate of the number of fibers for each type captured, it is essential to have the fiber-type section already scanned and the muscles reconstructed before starting the image acquisition of Bodipy-laminin (**Figure 3B**).

   1. For Bodipy image observation and acquisition, use a confocal microscope with a 40x oil immersion objective lens with a numerical aperture of 1.4.

   2. Use the following settings: pinhole at 1 AU, 2,048 pixel x 2,048 pixel resolution, pixel size at 0.08 µm,

unidirectional mode, scan speed at 4 (~4 μs/pixel), line averaging set to 4x, and digital zoom set to 1.

3. To avoid cross-talk between Bodipy-558/568 and laminin-AF647, use the sequential scan mode on the confocal software.

   NOTE: When the dye chosen is Bodipy-493/503, simultaneous confocal laser scanning is possible with no crosstalk between the Bodipy channel and laminin-AF647 channel. This will speed up the acquisition of images.

4. Excite Bodipy-493/503 using the 488 nm laser line or argon laser line, and excite Bodipy-555/568 using the 561 nm diode laser line. Finally, detect laminin-AF647 with a 640 nm diode laser line.

   CAUTION: Bear in mind that Bodipy molecules are very sensitive to photobleaching, so avoid unnecessary laser scanning. To recognize fibers, use only the laser for laminin.

5. Depending on the dye chosen, set the emission ranges at 570-650 nm for Bodipy-493/503[24] and at 565-620 nm for Bodipy-558/568. Set the emission range for laminin at 656-700 nm.

6. Set the gain and digital gain appropriately so no saturated pixels are detected on the range indicator. Correct the background signal by adjusting the offset.

   NOTE: Filter selection and other above-mentioned scanning parameters must be optimized for each confocal microscope. It is important that all the above-mentioned settings are kept constant for all the images captured from samples to be compared.

7. To identify the type of fiber among those visualized on the confocal microscope, use a personal laptop

on which the image of the section reconstructed after fiber-type immunodetection is checked (**Figure 3B**).

8. Once a group of fibers is correctly identified, acquire the image with the Bodipy and laminin channels.

   NOTE: It is recommended to note the Bodipy-laminin image name on the region of the muscle where these fibers are located on the image acquired for MyHC recognition to facilitate the later fiber-specific analysis of LDs.

## 6. Analysis of images

1. Analysis of the fiber-types on each muscle sample

   1. In Fiji (or ImageJ)[32], open the TIFF, PNG, or JPG file with the reconstructed muscle obtained from the merge of all the channels used to detect the fiber isoforms.

   2. To start the **Cell Counting** tool, click on **Plugins | Analyze | Cell counter | Cell counter**.

   3. On the **Cell counter** window, click on **Actions | Initialize**.

   4. Under **Counters** in the same window, select **Type 1**.

   5. On the Fiji main window, select the **Wand** tool.

   6. To quantify the number of fibers of each type, click on each fiber of the same type, so that the program records the number of fibers clicked.

   7. Once finished, select the next type of fiber and repeat the same steps.

   8. When all fibers of the image have been assigned to a given fiber type, click on **Results** on the **Cell Counter** window to display the results in a table.

   9. Save this table as a spreadsheet table by clicking on **File | Save As** on the **Results** window.

10. Save and reload the selections on the same image at any time by clicking on **Save Markers** or **Load Markers**, respectively, on the **Cell Counting** window.

2. Analysis of lipid droplets in a fiber-type-dependent manner

   1. Analyze the images of Bodipy and laminin obtained on the confocal using Fiji for the quantification of LDs.

      NOTE: The authors designed a customized macro to automatize the analysis. This macro, along with a step-by-step explanation on how to use it, is available as **Supplemental File 1** and **Supplemental File 2**, respectively.

   2. Open each image with the aid of the **Bio-Formats Importer** from Fiji. Under the **View Stack with** option, select **Hyperstack | Color mode, Default**. Make sure that the **Autoscale** window is selected.

      NOTE: The following steps will describe the protocol for the analysis of one fiber on the image, but it must be repeated as many times as the number of entire fibers appear on the image.

   3. Use the **freehand selection** tool to manually select the sarcolemma of the fiber based on the laminin channel (**Figure 4A**) and press T on the keyboard to record the selection or Region of Interest (ROI) on the **ROI** window.

   4. Go to Fiji's **main** window and click on **Analyze | Set Measurements**, and on the pop-up window, select **Area** and **Feret's diameter**. Leave the remaining boxes unchecked and other parameters as they appear by default.

5. Click on **Measure** on the **ROI** window to obtain the Area and Minimal Feret's Diameter (MF) of the fiber selected, and note them for later use.

   NOTE: When analyzing LDs, it is important to have in mind that their size and density vary between the center and the periphery (subsarcolemmal region-SS) of the fiber. Therefore, the analysis must be done separately.

6. Calculate the value of 1/6 of the MF to delimit the central part of the fiber.

   NOTE: In the macro, the default MF value is set to 6, which means that the reduction applied will be set as 1/6 of the MF. This value was chosen based on the empirical data obtained from the soleus of animals fed a high-fat diet. However, each researcher must change this number based on the empirical data and the muscle analyzed, the type of fiber, and the animal condition.

7. On the **ROI** window, click on **Add** to have a duplicate of the first ROI and select the second ROI that appears on the window.

8. On Fiji's main window, click on **Edit | Selection | Enlarge** and introduce the previously calculated value (from step 6.2.6.) with a minus sign before the number and click on **OK**. On the ROI window, click on **Add[t]** (a third ROI must appear) and **Delete**, to delete the second ROI.

   NOTE: The researcher can check the results by clicking on the **Show All** box on the **ROI** window. At this point, two ROIs must appear, one that surrounds the entire perimeter of the fiber (**Figure 4B**) and another one that is placed in the center (**Figure 4C**).

9. Select both ROIs on the **ROI** window and click on **More | XOR | Add[t]**. Wait for a third ROI to appear, which corresponds to the periphery of the fiber (**Figure 4D**).

10. Save the ROIs by clicking on **More | Save** to save the ROIs in case a later reanalysis of the same fibers is needed.

11. Select the **Bodipy channel** and open the **Threshold** tool by clicking on **Image | Adjust | Threshold** on Fiji's **main** window.

12. On the **Threshold** pop-up window, set the values to **70/255**, select **Yen | B&W method**, and click on **Dark background | Apply**.

    NOTE: The values applied on the **Threshold** may vary depending on the conditions of the experiment and the threshold must be appropriately set to optimize the analysis. A B&W window with the Bodipy signal above the threshold limit shown in white and the background in black must appear (compare the original Bodipy image in **Figure 4E** with the one in **Figure 4F**).

13. Go to Fiji's **main** window and click on **Analyze | Set Measurements** and on the pop-up window, select **Area, Area fraction,** and **Limit to threshold**. Leave the remaining boxes unchecked and other parameters as they appear by default.

    NOTE: If the researcher wants to analyze the "circularity" of LDs, which is an index of the spherical morphology that ranges from 1 for a perfect sphere to 0 for a line, click on the **Shape descriptors** box of the **Set Measurements** pop-up window.

14. Go to the **ROI** window and select the first ROI. On Fiji's **main** window, click on **Analyze | Analyze particles tool**.

    NOTE: This tool quantifies the number, size, area covered, and percentage of the total area covered by particles on each selection and saves the results as a spreadsheet file.

15. Set the values from **2** to **Infinity** (**2-Infinity**) on the **Analyze Particles** window, check the **Pixels** box, maintain the default circularity values, select **Summarize**, and click on **OK**.

    NOTE: To check the results on the fiber, under the **Show** option, select any of the available options. To have the information of each LD recognized on the selection in a table, check the **Display results** option on the **Analyze Particles** window. The results from the analysis of the total area of the fiber are averaged and summarized in a table with several columns (Count, Total Area, Average size, % Area; these correspond to the number of particles [LDs], the area occupied by these particles, their average size, and the percentage of the total area of the selection occupied by particles, respectively). To calculate the density, divide the number of particles by the total area of each selection.

16. To obtain the values of the center and the periphery of the fiber, repeat steps 6.2.14 and 6.2.15, selecting the second (center) and the third ROI (periphery) each time.

17. Save the results by clicking on **File | Save as** on the **Summary** window.

    NOTE: Include the type of fiber, the condition, and the image name on the assigned name of the results

to facilitate later unification and statistical analysis of the data. To analyze the rest of the fibers in the same image, repeat steps 6.2.3 to 6.2.17. For the statistical analysis, at least 10-15 fibers of each type must be analyzed per animal.

## Representative Results

The protocol described herein provides an efficient method to easily quantify LDs in a fiber type and subcellular-specific manner. It shows how, by freezing together two muscles of similar size, such as the EDL and the soleus, the time and resources spent on the following steps are reduced by half.

A complete protocol is provided for immunostaining, image acquisition, and analysis of the different MyHC isoforms expressed in adult mouse muscles. This protocol is based on the one first designed by Schiaffino et al. in 1989[33], with some adjustments such as the use of an additional antibody to label laminin. This later modification is critical for the location of type IIb fibers, which will be black as they are not stained with any antibody. As shown in **Figure 5**, this immunohistochemical protocol not only permits the recognition of mouse slow-oxidative (type I and IIa) and fast-glycolytic (type IIx and IIb) fibers, but also the presence of hybrid fibers (see asterisk in **Figure 5D**). Moreover, having the cross sections of both muscles on the same slide permits the comparison of the proportions of each fiber-type between the two selected muscles, ensuring that the experimental conditions were identical on both sections.

For LD labeling, the results presented here are based on the use of Bodipy-558/568 $C_{12}$ as a lipid dye; however, the reader is referred to an excellent protocol paper detailing the use of the classical dye Bodipy-493/503 on muscle sections[23]. The protocol presented combined the staining of LDs based on immunohistochemistry against α2-laminin to distinguish the fiber sarcolemma. As with the fiber-type experiment, this step is essential, not only for the recognition of individual fibers, but also for subsequent analysis of lipids in both the central and peripheral regions of fibers (**Figure 4**). One of the critical steps of this protocol is the identification and tagging of the same fibers on the two slides. As explained before, it is important to scan the slide with fiber types and have the reconstruction of muscle cross-sections with the merged colors before the acquisition of images for LDs (**Figure 3B**). Remarkable structures of each muscle section, such as axon twigs or muscle spindles, are good landmarks that could help the researcher locate the same fibers on both slides (**Figure 6**). Remember that because the slide is placed upside down on most confocal microscopes, it is recommended to invert the fiber-type-reconstructed image on the personal computer to facilitate the location task.

The settings described for the acquisition of Bodipy-laminin staining by confocal microscopy allow the visualization and later analysis of the size, number, and distribution of LDs from three to six fibers simultaneously (**Figure 6** and **Figure 7**). A detailed step-by-step protocol to analyze LDs with the image analysis software Fiji is also provided here. As shown in the protocol, the full analysis of each of the fibers present on an image is long and tedious. However, Fiji has the advantage of permitting the design of customized programs, called *macros*, based on the Java language. The authors designed a macro that enables the automation of the series of individual commands described above that is automatically run in a loop to analyze in a few minutes-not only each of the fibers present on an image but also a large set of images. The only input from the researcher is the manual selection of the perimeter of the fiber to be analyzed each time, the selection of the fiber

type, and the visual inspection of the resulting image after applying the threshold and quantifying the particles.

Here, the analysis of LDs in a location-dependent manner is implemented. By previously measuring the area and MF diameter of the fiber, a size-dependent (non-fixed as described by Strauss et al.[25]) reduction is applied to obtain the central and the peripheral areas of each fiber (**Figure 4** and **Figure 7**). As seen in the histograms of **Figure 7**, this method allows the quantification of three important parameters: the percentage of the fiber area occupied by LDs (**Figure 7E**), the density of LDs-the number of LDs per $\mu m^2$ (**Figure 7F**), and the average size of LDs (**Figure 7G**). As a result, in 3-month-old mice (N = 5), type IIa (green outline) and type IIx (red outline) fibers present the largest proportion of area occupied by LDs in the periphery (**Figure 7E**). With respect to the density of particles, EDL fibers always show higher density than soleus fibers independently of the subcellular location (**Figure 7F**). Finally, the average size of those LDs is always larger in the periphery than in the center (**Figure 7G**).

The different methods used by other groups to assess the accumulation of LDs in rodent skeletal muscle[34,35] make it difficult to compare these results with those of previous studies. However, in line with the results from Komiya et al.[34], the percentage of fiber area occupied by LDs is higher in soleus type IIa and EDL type IIx fibers. Most importantly, type IIb fibers presented the lowest percentage of area occupied by LDs (**Figure 7E**, grey histograms). Since fiber type IIb is the most predominant fiber type of the EDL (75%, **Figure 5E**), these results confirm what other groups have previously described: the overall accumulation of lipids is lower in EDL than in the soleus[34,35].

Contrary to what has been described in humans[25], and also in line with the results of Komiya et al.[34], the results presented here show that the accumulation of LDs in soleus type I fibers is relatively low. This could be explained by fiber-type interspecies differences between mice and humans[36], since the metabolic properties of human type I fibers are more similar to those of rodent type IIa and IIx, while those of human type IIx fibers are close to rodent type IIb[37]. In summary, the different techniques described here provide a reproducible, reliable, and time-efficient method to study and compare several parameters related to LDs and their distribution within the cell in a fiber type-dependent manner.

**Suboptimal experiments**

If the freezing procedure is not performed correctly and isopentane is not at the right temperature, **ice crystals** will form inside the fibers (**Figure 8A**). These freezing artifacts are detectable only after the histological preparation of the sample and can be recognized as holes in the fibers. For proper quantification of LDs, these artifacts must be avoided. It has been demonstrated that thawing and refreezing the muscle block appropriately can significantly reduce these artifacts[29].

Another problem is encountered when **fibers are not cut perpendicular to the longitudinal axis** (**Figure 8B**). LD quantification and comparison between fibers, muscles, or animals cannot be done when sections are not transverse. For this reason, it is essential to place the muscles correctly on the cork with the aid of a stereo microscope before freezing and have a brightfield microscope close to the cryostat. The latter will allow the researcher to find the correct alignment of the sample on the cryostat.

In some rare occasions, the **labeling of MyHC isoforms is very weak** on one or more fiber types (**Figure 8C**). If

this happens, the analysis of LDs will be incomplete. In this case, the experiment has to be repeated starting from the cutting of the muscles. Finally, **Bodipy could accumulate in the periphery of the muscle cross section** (**Figure 8D**). If

this happens, the staining will be very strong on those fibers producing an artifactual result. Avoid the acquisition of images from these fibers.
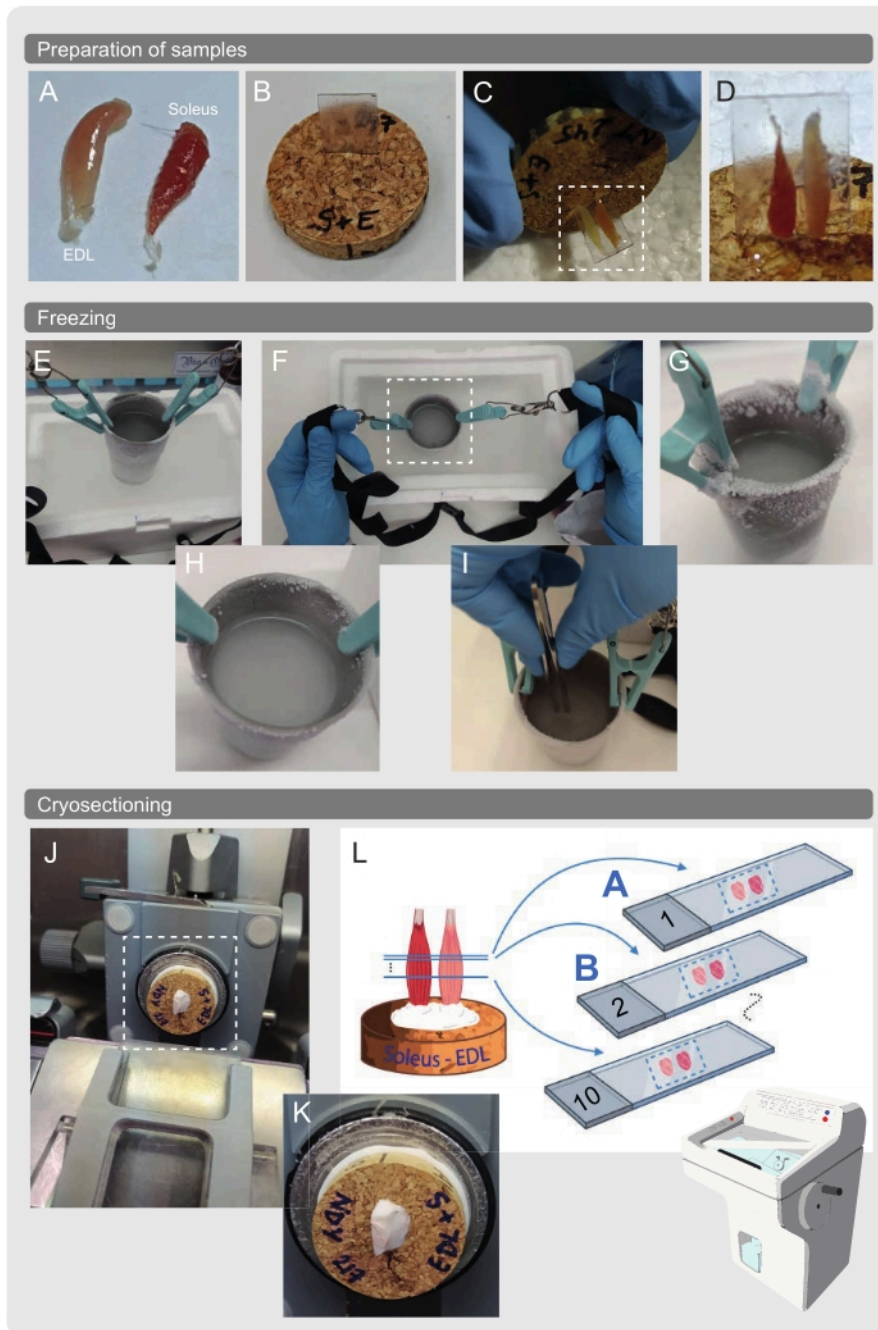
**Figure 2: Preparation of the samples for freezing and cryosectioning.** (**A-D**) Mouse soleus and EDL muscles are dissected and placed on a cork held by a rigid plastic with a drop of OCT. (**E-G**) A stainless steel tumbler is filled with isopentane and cooled to its melting temperature in liquid nitrogen. (**H,I**) The tumbler with the cold isopentane is taken out of the liquid nitrogen, and the sample is immersed up to the bottom of the tumbler, swirling for 15 s. (**J-L**) The cork with the samples is placed on the cryostat holder disk without the plastic support, and serial transverse sections of 10 µm are directly mounted on adhesion slides. Two adjacent serial cross-sections are immediately processed for the staining of LDs and the detection of MyHCs. Abbreviations: LDs = lipid droplets; EDL = extensor digitorum longus; MyHCs = myosin heavy chain isoforms; OCT = optimum cutting temperature. Please click here to view a larger version of this figure.
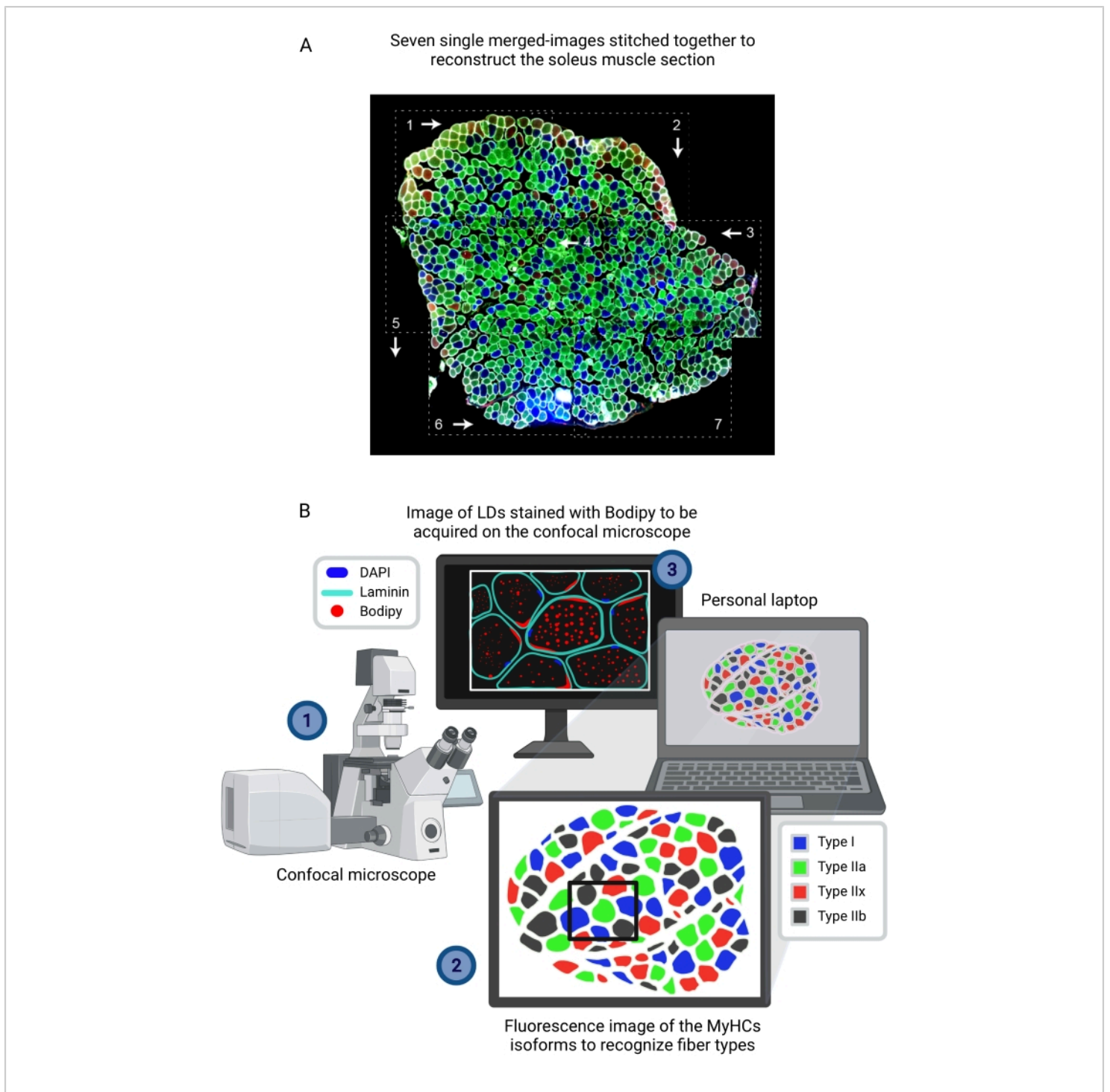
**Figure 3: Bodipy image acquisition after identifying the type of fiber from the reconstructed composite image seen on another computer.** (**A**) Reconstruction of the entire soleus section immunolabeled for fiber type (MyHCs) from seven independent merged images (dashed rectangles) stitched together using image processing software. The white arrows and the numbers represent the order followed during image acquistion using a conventional epifluorescence microscope. (**B**) For Bodipy image acquisition, (**1**) a field containing the muscle section immunostained with laminin-AF647 and Bodipy-555/568

is visualized on the screen of a computer connected to the confocal microscope. (**2**) Those fibers are located on the reconstructed image of the muscle section immunostained to detect the type of fibers (MyHCs). (**3**) The image is acquired using a confocal microscope. Abbreviations: LDs = lipid droplets; DAPI = 4',6-diamidino-2-phenylindole; MyHCs = myosin heavy chain isoforms. Please click here to view a larger version of this figure.
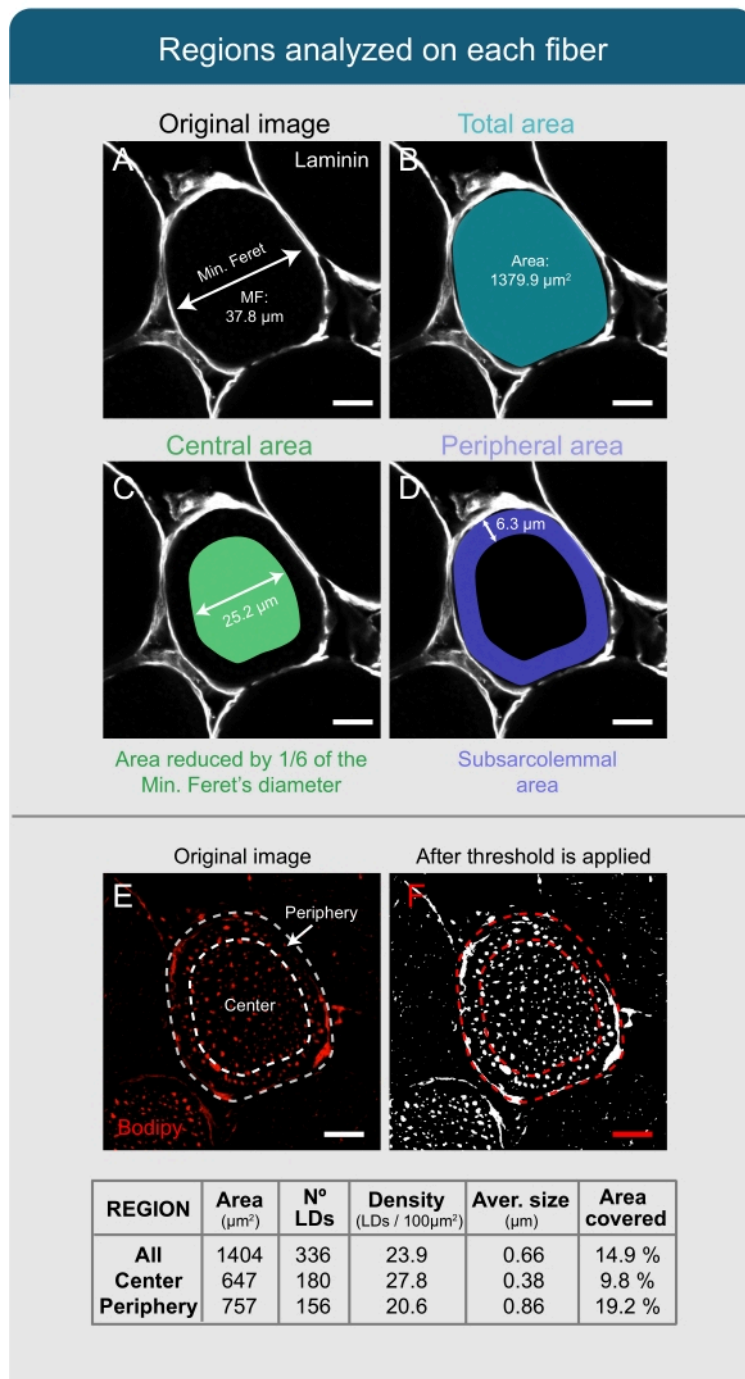
**Figure 4: Analysis of lipid droplets with Fiji. (A,B)** The sarcolemma of the fiber is recognized based on the laminin image and selected as the ROI. Total area and MF are measured. **(C)** To recognize the central part of the fiber, the selection is reduced by 1/6 of the value of the MF. **(D)** The area between the central and the total selection is set as the periphery or the subsarcolemmal area. **(E)** For the analysis of LDs stained with Bodipy, a threshold is applied, **(F)** and the **Analyze Particles** tool is used to quantify different parameters related to the LDs (see table). These values are obtained for the complete

fiber (All), for the central part (Center), and for the subsarcolemmal area (Periphery), independently. Scale bars = 12 μm. Abbreviations: LDs = lipid droplets; ROI = region of interest; MF = Minimal Feret's diameter. Please click here to view a larger version of this figure.
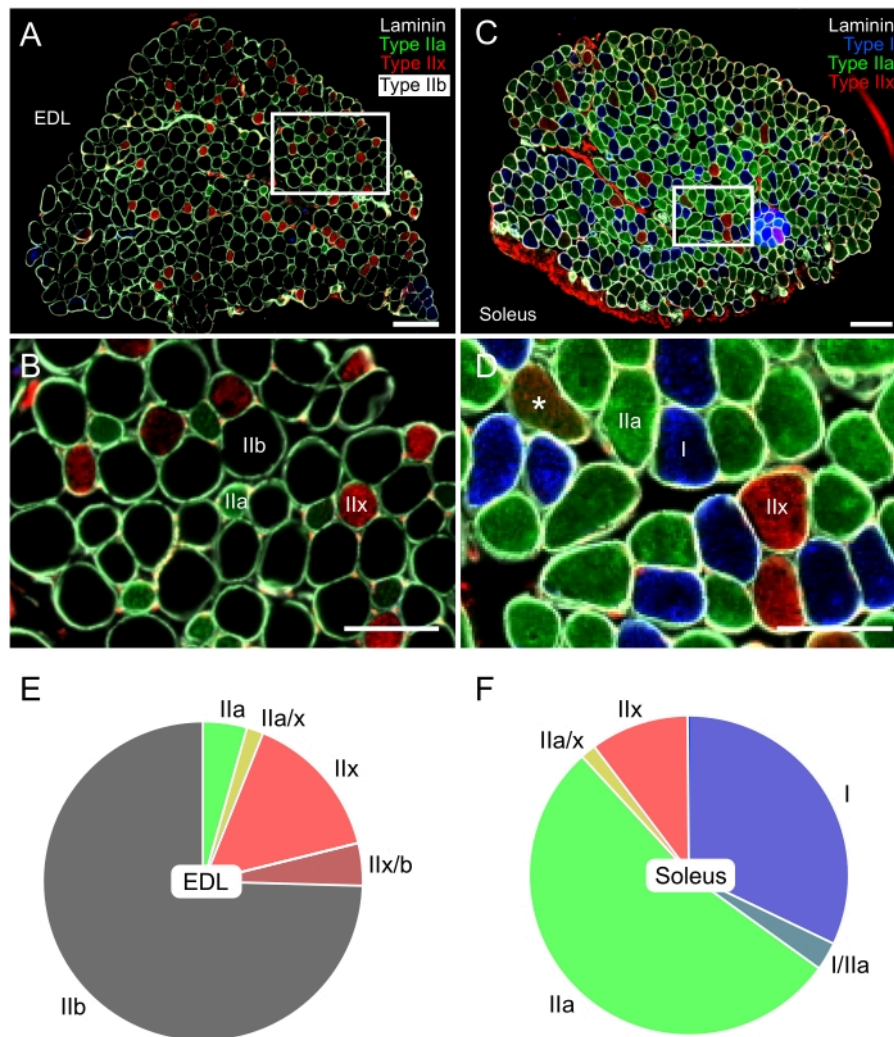
**Figure 5: Representative immunostaining of fiber types in EDL (glycolytic) and soleus (oxidative) mouse muscle.**
Merged fluorescence images of EDL (**A**,**B**) and soleus (**C**,**D**) obtained with a digital, whole-slide fluorescence microscope. Antibodies against type I (blue-AF405), type IIa (green-AF488), type IIx (red-AF568), and laminin (white-AF647) were used. Black fibers correspond to fiber type IIb. **B** and **D** show details of the fibers inside the white rectangles of panels **A** and **C**, respectively. The asterisk (*) in panel **D** shows a IIa/IIx hybrid fiber. (**E**,**F**) Representative quantification of fiber type distribution in EDL and soleus from 3-month-old mice (N = 5). EDL was mainly composed of type IIb, then IIx, and IIa fibers (~75%, 15%, and 5%, respectively). By contrast, soleus was mainly composed of type IIa (>50%) and type I fibers (30%). The proportions of type IIx fibers were rather similar in both muscles, while those of hybrid fibers were very low. Scale bars = 200 µm (**A,C**), 100 µm (**B,D**). Abbreviation: EDL = extensor digitorum longus. Please click here to view a larger version of this figure.
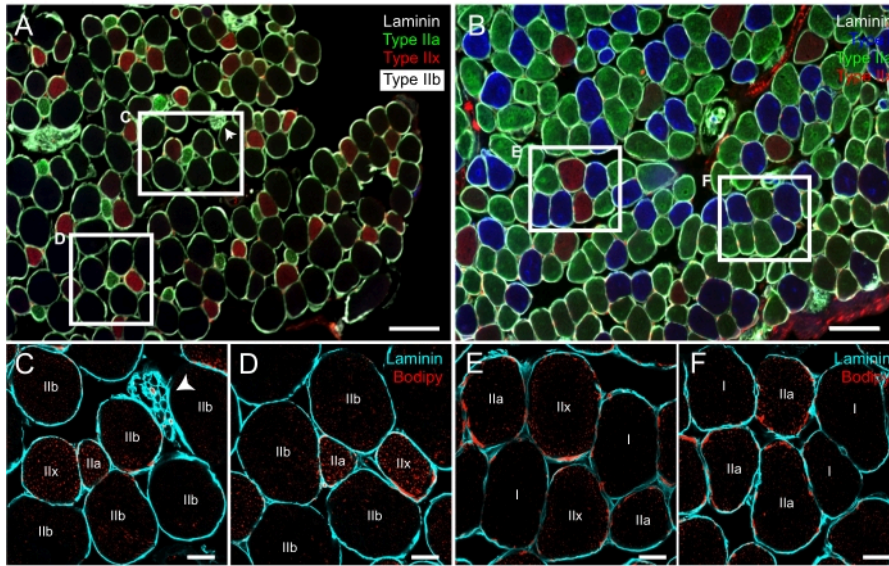
**Figure 6: Representative staining of LDs with Bodipy on serial cross sections previously immunolabeled for MyHC isoforms.** Fluorescence merged images of mouse EDL (**A**) and soleus (**B**) acquired using an epifluorescence microscope showing type I (blue), IIa (green), IIx (red), IIb (black) fibers, and laminin (white signal surrounding the fibers). (**C-F**) Confocal fluorescence images from the EDL (**C,D**) and the soleus (**E,F**) co-labeled with laminin (cyan) and Bodipy (red). Note that fibers shown in **C-F** are the same as those inside the white rectangles on panels **A** and **B**. On the right corner of the white rectangle in **A**, an axon twig can be distinguished (white arrowhead). Scale bars = 200 µm (**A,B**), 20 µm (**C-F**). Abbreviations: LDs = lipid droplets; EDL = extensor digitorum longus; MyHCs = myosin heavy chain isoforms. Please click here to view a larger version of this figure.
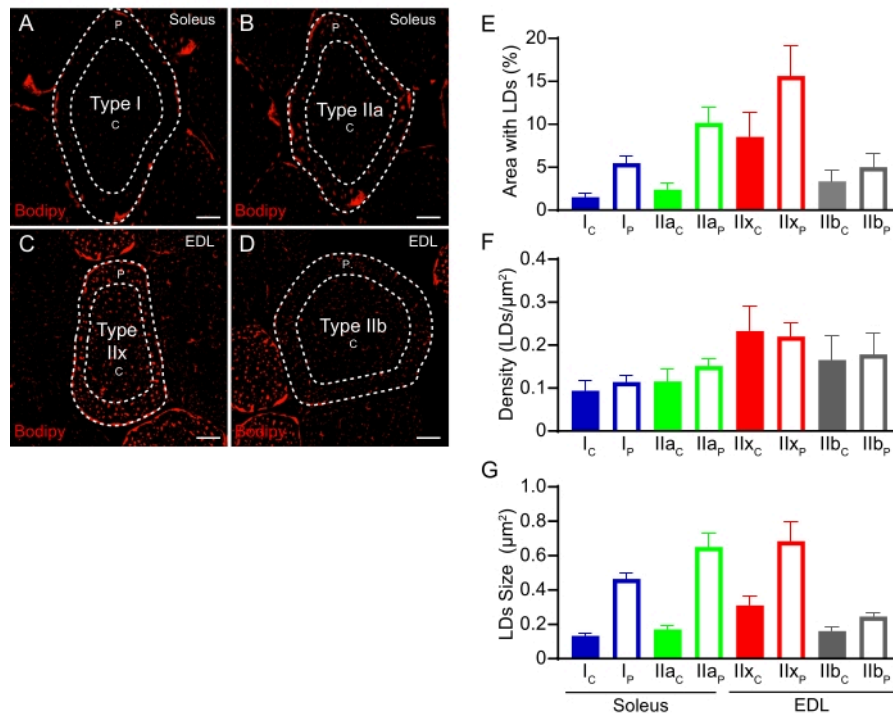
**Figure 7: Quantification of LDs in a fiber-type- and subcellular-specific manner.** Representative fluorescence confocal images of type I and type IIa fibers from soleus (**A,B**) and type IIx and type IIb fibers from EDL (**C,D**) obtained after co-labeling with Bodipy (red) and α2-laminin (not shown). LD content (% of the area occupied by Bodipy and density) and morphology (size) were analyzed in a subcellular-specific manner. Fiber perimeter was defined by laminin staining and the central or peripheral areas were set based on the MF diameter. Percentage of fiber area occupied by Bodipy (LDs) (**E**), LD density (number/µm$^2$) (**F**), or average LD size (**G**) in central or peripheral regions for each fiber type. Results are represented as mean ± SEM. Scale bars = 10 µm. Abbreviations: LDs = lipid droplets; EDL = extensor digitorum longus; C = central; P = peripheral. Please click here to view a larger version of this figure.
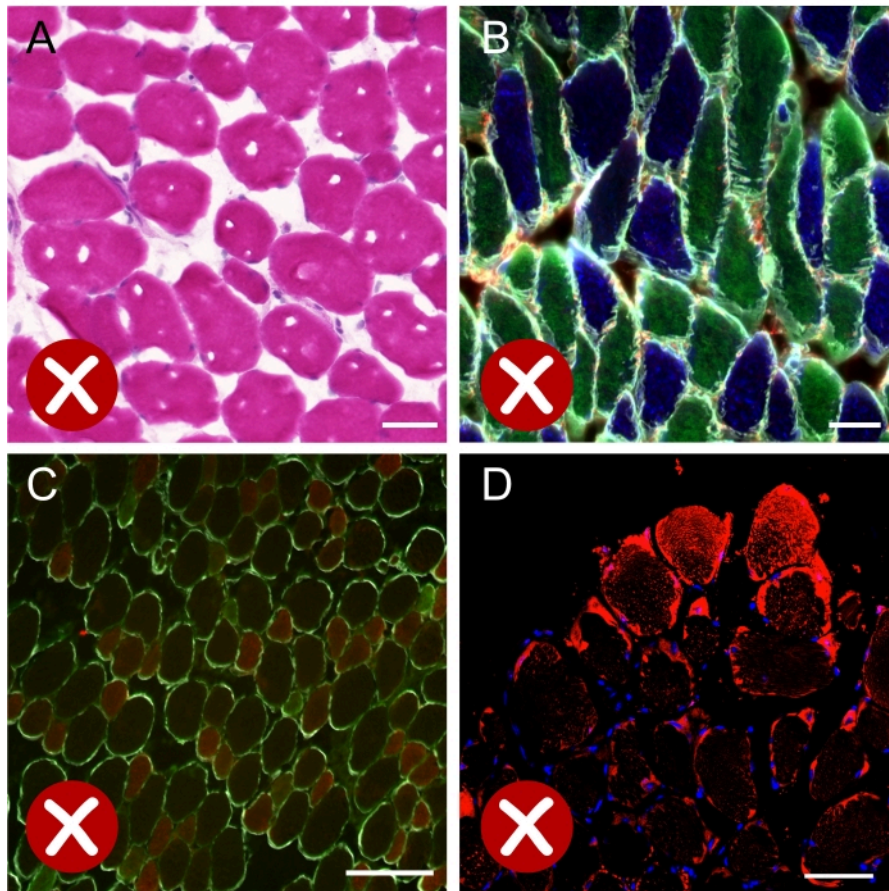
**Figure 8: Images corresponding to suboptimal results.** (**A**) Brightfield image of muscle cross-section stained for hematoxylin-eosin showing ice crystals formed during the freezing process. (**B**) Fluorescence merged image of a soleus section immunostained for MyHCs and laminin, showing that the majority of fibers are cut along the longitudinal axis. (**C**) Fluorescence image of an EDL section immunostained for MyHCs and laminin. The weak staining of fiber type IIa (green) hinders the correct quantification of each fiber type. (**D**) Confocal image showing a strong artifactual staining of Bodipy (red) on fibers located at the periphery of the muscle cross section. Scale bars = 50 μm (**A,B**), 200 μm (**C,D**). Abbreviations: EDL = extensor digitorum longus; MyHCs = myosin heavy chain isoforms. Please click here to view a larger version of this figure.

**Supplemental Figure S1: LD staining with Oil Red O on muscle cross sections.** (**A,B**) Confocal images showing the pattern of staining obtained with Oil Red O in the soleus and EDL, respectively. The protocol used for this staining is described in detail by Prats et al.[24]. Note that accumulation of LDs is higher in the subsarcolemmal region of the myofibers,

as previously described for Bodipy. Scale bars = 20 μm. Abbreviations: LD = lipid droplet; EDL = extensor digitorum longus. Please click here to download this File.

**Supplemental Figure S2: Co-staining of LDs and mitochondria in the soleus muscle.** (**A**) Confocal merged image showing the immunolabeling of Tomm20, a protein

present on the mitochondrial membrane (green), DAPI (blue), and Bodipy-558/568 labeled LDs (red). The inset in **A** shows several mitochondria (green) bound to LDs (red). This image was obtained by applying Airyscan confocal superresolution microscopy. (**B**,**C**) Corresponding single-channel images of LDs and mitochondria, respectively. Scale bars = 10 µm (**A-C**), 5 µm (**A, inset**). Abbreviations: LDs = lipid droplets; DAPI = 4',6-diamidino-2-phenylindole. Please click here to download this File.

**Supplemental File 1:** Fiji macro for the automated analysis of LDs on multiple laminin+Bodipy images. Please click here to download this File.

**Supplemental File 2:** Step-by-step explanation of how to work with the macro Bodipy_JoVE.ijm. Please click here to download this File.

## Discussion

The protocol detailed here describes an efficient method to quantify LDs tagged with Bodipy on a fiber-type- and subcellular-specific basis. In recent years, classical lipid dyes, such as ORO or Sudan Black B, have been substituted with a new array of cell-permeable, lipophilic, fluorescent dyes that bind to neutral lipids (e.g., Bodipy). Available as different conjugates, Bodipy has been proven very effective at tagging LDs to study their morphology, dynamics, and interaction with other organelles, not only in different fixed tissues and cells[23,38,39,40] but also in living cells[41,42].

Within the protocol, there are several critical aspects that the researcher must consider to obtain optimal results. It is essential to place the chosen muscles correctly on the cork to ensure perfect alignment and orientation of muscle myofibers, since once frozen, only slight readjustments of the holder can be made on the cryostat. Moreover, it is critical to start

the immunostaining protocol immediately after the sections are cut, since air-drying cryosections (for only 15 min) has severe adverse effects on LDs, resulting in a 66% decrease in LD density and a 37% decrease in the average size[24]. Similarly, freezing and thawing the slides would have adverse effects and are therefore not recommended. A third important feature of this protocol is related to the fixation of samples. For the identification of the different MyHC isoforms with the antibodies cited here, tissue fixation must be avoided as it disrupts the binding of the chosen antibodies to their epitopes. If the muscle samples have been previously fixed, the reader is referred to a recently published paper using different antibodies[43]. Only PFA without methanol is recommended for the labeling and quantification of LDs, because the use of methanol or acetone disrupts the morphology of LDs[23,44]. Furthermore,a permeabilization step is not necessary for the quantification of LDs on slides immunolabeled with laminin. Since some groups have shown that permeabilization with detergents such as TritonX-100, saponin, or glycine can reduce the size or number of LDs[44,45], permeabilization is highly discouraged. Finally, the fine-tuning of the confocal microscope settings is crucial to recognize only the neutral lipids present in LDs and not those in membranes of other organelles[24].

Here, Bodipy-558/568 $C_{12}$ was used as a LD marker. However, the most frequently Bodipy used for tagging LDs and studying their morphology and location within the skeletal muscle myofibers is Bodipy-493/503. Both dyes are similar in their incubation time, working concentration, and their narrow emission spectra, although their excitation and emission ranges are slightly different. For a complete protocol on the use of Bodipy-493/503, the reader is referred to the work of Listenberger and Brown[46] or Spangenburg et al.[23]. Bodipy-558/568 $C_{12}$ has been used

for staining LDs in other tissues such as adipose tissue[47], degenerating retina[48], fibrotic kidneys[49], or fibroblasts[50]. This Bodipy yields a similar staining to the one obtained with ORO (see **Supplemental Figure S1**) but with considerably less technical burden and more specificity[24,51]. Moreover, Bodipy-558/568 C$_{12}$ has the advantage of enabling the quantification of LDs in combination with the detection of proteins or organelles tagged with a green-spectrum secondary antibody (see **Supplemental Figure S2** and Yan et al.[49]) or with GFP-genetically modified models[52]. These two applications are very powerful tools to unravel the dynamics and interactions of LDs with other cell organelles and proteins. Nevertheless, when no colabeling of proteins within the cells is intended, the authors recommend the use of the best-characterized LD dye Bodipy-493/503.

One of the limitations of this protocol is related to the acquisition of images and the quantification of LD morphological characteristics. Technological advances in confocal laser scanning microscopy have greatly improved the plane resolution compared with wide-field microscopes and permit 3D reconstruction of objects when scanning the sample in the Z plane. This has been very useful for the study of LD morphology[24] and interaction with other proteins in skeletal myofibers[38,53], but has increased the image acquisition and processing time, since each 3D-reconstructed image is composed of several independent 2D images. In the above protocol, confocal images were acquired with a 40x objective lens and only in 2D. This method allows the acquisition of three to six myofibers per image instead of only one as it would be when using a 63x objective. This results in lower resolution and an overall estimation of the LD size and morphology that is not completely accurate. Nevertheless, it permits the analysis of a greater number of fibers per sample, which is also an important fact to consider, especially in

animal experiments, in which a high number of muscles and conditions must be compared.

Here, it is shown that, by freezing two muscles of similar size that are adjacent to each other[34], the processing time of the samples is considerably decreased, and possible artifactual differences derived from their independent processing are reduced. Moreover, this method of analyzing LDs takes into consideration the differences between the subcellular distribution of LDs within and among fiber types[54]. Selecting the perimeter of the myofiber and reducing this selection in relation to the fiber's Minimal Feret's diameter facilitates the study of the size and density of central and peripheral (subsarcolemmal) LDs independently. Applying this method is extremely important since it has been demonstrated that the subsarcolemmal accumulation of LDs directly contributes to insulin resistance. While some reports in humans have studied LDs in a fiber type- and location-dependent fashion[11,16,25], this is the first time, to our knowledge, that this method has been applied to muscles from rodents. Moreover, the quantification of LDs with the aid of a self-designed macro for Fiji significantly reduced and simplified the image analysis time. Both the macro and a step-by-step explanation on how to use it are available as **Supplemental File 1** and **Supplemental File 2**, respectively.

Overall, the authors consider that the protocol described herein could be a useful tool for other researchers studying lipid metabolism in skeletal muscle. The techniques explained may be applied to different muscles and under distinct conditions (fasted/overfed, trained/sedentary, young/aged, lean/obese) and will hopefully help to better comprehend the dynamics of LDs, the importance of their interactions with other components of the cell, how lipids are stored and

metabolized in glycolytic and oxidative fibers, and their role in the onset of insulin resistance in type 2 diabetes.

## Disclosures

The authors have no conflicts of interest to declare.

## Acknowledgments

## References

1. Correa-de-Araujo, R. et al. Myosteatosis in the context of skeletal muscle function deficit: an interdisciplinary workshop at the National Institute on Aging. *Frontiers in Physiology.* **11**, 963 (2020).

2. Miljkovic, I. et al. Greater skeletal muscle fat infiltration is associated with higher all-cause and cardiovascular mortality in older men. *Journals of Gerontology Series A: Biomedical Sciences and Medical Sciences.* **70** (9), 1133-1140 (2015).

3. Nachit, M. et al. Myosteatosis rather than sarcopenia associates with non-alcoholic steatohepatitis in non-alcoholic fatty liver disease preclinical models. *Journal of Cachexia, Sarcopenia, and Muscle.* **12** (1), 144-158 (2021).

4. Aleixo, G. F. P. et al. Myosteatosis and prognosis in cancer: Systematic review and meta-analysis. *Critical Reviews in Oncology/Hematolgoy.* **145**, 102839 (2020).

5. Gemmink, A., Schrauwen, P., Hesselink, M. K. C. Exercising your fat (metabolism) into shape: a muscle-centred view. *Diabetologia.* **63** (8), 1453-1463 (2020).

6. van Loon, L. J. Use of intramuscular triacylglycerol as a substrate source during exercise in humans. *Journal of Applied Physiology.* **97** (4), 1170-1187 (2004).

7. Coen, P. M., Goodpaster, B. H. Role of intramyocelluar lipids in human health. *Trends in Endocrinology and Metabolism.* **23** (8), 391-398 (2012).

8. Seibert, J. T., Najt, C. P., Heden, T. D., Mashek, D. G., Chow, L. S. Muscle lipid droplets: cellular signaling to exercise physiology and beyond. *Trends in Endocrinology and Metabolism.* **31** (12), 928-938 (2020).

9. Bergman, B. C., & Goodpaster, B. H. Exercise and muscle lipid content, composition, and localization: influence on muscle insulin sensitivity. *Diabetes.* **69** (5), 848-858 (2020).

10. Nielsen, J., Christensen, A. E., Nellemann, B., Christensen, B. Lipid droplet size and location in human skeletal muscle fibers are associated with insulin sensitivity. *American Journal of Physiology-*

*Endocrinology and Metabolism.* **313** (6), E721-E730 (2017).

11. Covington, J. D. et al. Intramyocellular lipid droplet size rather than total lipid content is related to insulin sensitivity after 8 weeks of overfeeding. *Obesity (Silver Spring).* **25** (12), 2079-2087 (2017).

12. Bosma, M. Lipid droplet dynamics in skeletal muscle. *Experimental Cell Research.* **340** (2), 180-186 (2016).

13. Nielsen, J. et al. Increased subsarcolemmal lipids in type 2 diabetes: effect of training on localization of lipids, mitochondria, and glycogen in sedentary human skeletal muscle. *American Journal of Physiology-Endocrinology and Metabolism.* **298** (3), E706-713 (2010).

14. Ferreira, R. et al. Subsarcolemmal and intermyofibrillar mitochondria proteome differences disclose functional specializations in skeletal muscle. *Proteomics.* **10** (17), 3142-3154 (2010).

15. Barrett, J. S., Whytock, K. L., Strauss, J. A., Wagenmakers, A. J. M., Shepherd, S. O. High intramuscular triglyceride turnover rates and the link to insulin sensitivity: influence of obesity, type 2 diabetes and physical activity. *Applied Physiology, Nutrition and Metabolism.* 1-14 (2022).

16. Daemen, S. et al. Distinct lipid droplet characteristics and distribution unmask the apparent contradiction of the athlete's paradox. *Molecular Metabolism.* **17**, 71-81 (2018).

17. Bredella, M. A., Ghomi, R. H., Thomas, B. J., Miller, K. K., Torriani, M. Comparison of 3.0 T proton magnetic resonance spectroscopy short and long echo-time measures of intramyocellular lipids in obese and normal-weight women. *Journal of Magnetic Resonance Imaging.* **32** (2), 388-393 (2010).

18. Schrauwen-Hinderling, V. B., Hesselink, M. K., Schrauwen, P., Kooi, M. E. Intramyocellular lipid content in human skeletal muscle. *Obesity (Silver Spring).* **14** (3), 357-367 (2006).

19. De Bock, K. et al. Evaluation of intramyocellular lipid breakdown during exercise by biochemical assay, NMR spectroscopy, and Oil Red O staining. *American Journal of Physiology-Endocrinology and Metabolism.* **293** (1), E428-434 (2007).

20. Koopman, R., Schaart, G., Hesselink, M. K. Optimisation of oil red O staining permits combination with immunofluorescence and automated quantification of lipids. *Histochemistry and Cell Biology.* **116** (1), 63-68 (2001).

21. Gueugneau, M. et al. Skeletal muscle lipid content and oxidative activity in relation to muscle fiber type in aging and metabolic syndrome. *Journal of Gerontology Series A: Biomedical Sciences and Medical Sciences.* **70** (5), 566-576 (2015).

22. Gemmink, A. et al. Super-resolution microscopy localizes perilipin 5 at lipid droplet-mitochondria interaction sites and at lipid droplets juxtaposing to perilipin 2. *Biochimica et Biophysica Acta-Molecular and Cell Biology of Lipids.* **1863** (11), 1423-1432 (2018).

23. Spangenburg, E. E., Pratt, S. J. P., Wohlers, L. M., Lovering, R. M. Use of BODIPY (493/503) to visualize intramuscular lipid droplets in skeletal muscle. *Journal of Biomedicine and Biotechnology.* 598358 (2011).

24. Prats, C. et al. An optimized histochemical method to assess skeletal muscle glycogen and lipid stores reveals two metabolically distinct populations of type I muscle fibers. *PLoS One.* **8** (10), e77774 (2013).

25. Strauss, J. A., Shepherd, D. A., Macey, M., Jevons, E. F. P., Shepherd, S. O. Divergence exists in the subcellular distribution of intramuscular triglyceride in human skeletal muscle dependent on the choice of lipid dye. *Histochemistry and Cell Biology.* **154** (4), 369-382 (2020).

26. Shepherd, S. O. et al. Sprint interval and traditional endurance training increase net intramuscular triglyceride breakdown and expression of perilipin 2 and 5. *Journal of Physiology.* **591** (3), 657-675 (2013).

27. Whytock, K. L. et al. A 7-day high-fat, high-calorie diet induces fibre-specific increases in intramuscular triglyceride and perilipin protein expression in human skeletal muscle. *Journal of Physiology.* **598** (6), 1151-1167 (2020).

28. Wang, C., Yue, F., Kuang, S. Muscle histology characterization using h&e staining and muscle fiber type classification using immunofluorescence staining. *Bio-Protocol.* **7** (10) (2017).

29. Meng, H. et al. Tissue triage and freezing for models of skeletal muscle disease. *Journal of Visualized Experiments: JoVE.* (89) (2014).

30. Kumar, A., Accorsi, A., Rhee, Y., Girgenrath, M. Do's and don'ts in the preparation of muscle cryosections for histological analysis. *Journal of Visualized Experiments: JoVE.* (99), e52793 (2015).

31. Leiva-Cepas, F. et al. Laboratory methodology for the histological study of skeletal muscle. *Archivos de Medicina del Deporte.* **35** (186), 254-262 (2018).

32. Schindelin, J. et al. Fiji: an open-source platform for biological-image analysis. *Nature Methods.* **9** (7), 676-682 (2012).

33. Schiaffino, S. et al. Three myosin heavy chain isoforms in type 2 skeletal muscle fibres. *Journal of Muscle Research & Cell Motility.* **10** (3), 197-205 (1989).

34. Komiya, Y. et al. Mouse soleus (slow) muscle shows greater intramyocellular lipid droplet accumulation than EDL (fast) muscle: fiber type-specific analysis. *Journal of Muscle Research & Cell Motility.* **38** (2), 163-173 (2017).

35. Andrich, D. E. et al. Altered lipid metabolism impairs skeletal muscle force in young rats submitted to a short-term high-fat diet. *Frontiers in Physiology.* **9**, 1327 (2018).

36. Schiaffino, S. Fibre types in skeletal muscle: a personal account. *Acta Physiologica.* **199** (4), 451-463 (2010).

37. Bloemberg, D., Quadrilatero, J. Rapid determination of myosin heavy chain expression in rat, mouse, and human skeletal muscle using multicolor immunofluorescence analysis. *PLoS One.* **7** (4), e35273 (2012).

38. Gemmink, A. et al. Decoration of intramyocellular lipid droplets with PLIN5 modulates fasting-induced insulin resistance and lipotoxicity in humans. *Diabetologia.* **59** (5), 1040-1048 (2016).

39. Askinas, C. et al. in *Biophotonics Congress: Biomedical Optics Congress 2018 (Microscopy/Translational/Brain/OTS).* JTu3A.4 (Optical Society of America) (2018).

40. Morén, B. et al. EHD2 regulates adipocyte function and is enriched at cell surface-associated lipid droplets in primary human adipocytes. *Molecular Biology of the Cell.* **30** (10), 1147-1159 (2019).

41. Benador, I. Y. et al. Mitochondria bound to lipid droplets have unique bioenergetics, composition, and dynamics that support lipid droplet expansion. *Cell Metabolism.* **27** (4), 869-885.e866 (2018).

42. de la Rosa Rodriguez, M. A. et al. Hypoxia-inducible lipid droplet-associated induces DGAT1 and promotes lipid storage in hepatocytes. *Molecular Metabolism.* **47**, 101168 (2021).

43. Jevons, E. F. P., Gejl, K. D., Strauss, J. A., Ørtenblad, N., Shepherd, S. O. Skeletal muscle lipid droplets are resynthesized before being coated with perilipin proteins following prolonged exercise in elite male triathletes. *American Journal of Physiology-Endocrinology and Metabolism.* **318** (3), E357-E370, (2020).

44. Ohsaki, Y., Maeda, T., Fujimoto, T. Fixation and permeabilization protocol is critical for the immunolabeling of lipid droplet proteins. *Histochemistry and Cell Biology.* **124** (5), 445-452 (2005).

45. Prats, C. et al. Decrease in intramuscular lipid droplets and translocation of HSL in response to muscle contraction and epinephrine. *Journal of Lipid Research.* **47** (11), 2392-2399 (2006).

46. Listenberger, L. L., Brown, D. A. Fluorescent detection of lipid droplets and associated proteins. *Current Protocols in Cell Biology.* **Chapter 24** (Unit 24.22) (2007).

47. Xue, Y., Lim, S., Bråkenhielm, E., Cao, Y. Adipose angiogenesis: quantitative methods to study microvessel growth, regression and remodeling in vivo. *Nature Protocols.* **5** (5), 912-920 (2010).

48. Muliyil, S. et al. ADAM17-triggered TNF signalling protects the ageing Drosophila retina from lipid droplet-mediated degeneration. The *EMBO Journal.* **39** (17), e104415 (2020).

49. Yan, Q. et al. Autophagy activation contributes to lipid accumulation in tubular epithelial cells during kidney fibrosis. *Cell Death Discovery.* **4**, 2 (2018).

50. Coassin, S. et al. Investigation and functional characterization of rare genetic variants in the adipose triglyceride lipase in a large healthy working population. *PLoS Genetics.* **6** (12), e1001239 (2010).

51. Daemen, S., van Zandvoort, M., Parekh, S. H., Hesselink, M. K. C. Microscopy tools for the investigation of intracellular lipid storage and dynamics. *Molecular Metabolism.* **5** (3), 153-163 (2016).

52. Chen, Q. et al. Rab8a deficiency in skeletal muscle causes hyperlipidemia and hepatosteatosis by impairing muscle lipid uptake and storage. *Diabetes.* **66** (9), 2387-2399 (2017).

53. Gemmink, A. et al. Decoration of myocellular lipid droplets with perilipins as a marker for in vivo lipid droplet dynamics: A super-resolution microscopy study in trained athletes and insulin resistant individuals. *Biochimica et Biophysica Acta (BBA)-Molecular and Cell Biology of Lipids.* **1866** (2), 158852 (2021).

54. Bergman, B. C., Hunerdosse, D. M., Kerege, A., Playdon, M. C., Perreault, L. Localisation and composition of skeletal muscle diacylglycerol predicts insulin resistance in humans. *Diabetologia.* **55** (4), 1140-1150 (2012).